2009-10-26

In-Plane All-Photonic Transduction with Differential Splitter Using Double-Step Rib Waveguide for Photonic Microcantilever Arrays

Ryan Anderson
rra2@byu.net

Seunghyun Kim

Gregory P. Nordin
nordin@byu.edu

Jong Wook Noh

Weisheng Hu

Original Publication Citation

J.W. Noh, R. Anderson, S. Kim, W. Hu, G.P. Nordin, "In-plane all-photonic transduction with differential splitter using double-step rib waveguide for photonic microcantilever arrays," Opt. Express 17(22), pp. 212-22 (29). http://www.opticsinfobase.org/oe/abstract.cfm?uri=oe-17-22-212.

In-plane all-photonic transduction with differential splitter using double-step rib waveguide for photonic microcantilever arrays

Jong Wook Noh, Ryan R. Anderson, Seunghyun Kim, Weisheng Hu, and Gregory P. Nordin*

Department of Electrical and Computer Engineering, Brigham Young University, Provo, Utah 84602
**nordin@byu.edu*

Abstract: We report a differential splitter consisting of an asymmetric double-step multimode rib waveguide and a Y-branch splitter for in-plane photonic transduction of photonic microcantilever deflection. Arrays of photonic microcantilevers are integrated with differential splitters and an optical waveguide network to demonstrate uniformity and sensitivity of transduction. Measurement results from multiple arrays indicate a sensitivity of 0.32×10^{-3} nm^{-1} and minimum detectable deflection of 141 pm for a 3.5 Hz measurement bandwidth.

OCIS codes: (120.6010) Sensors; (120.3120) Integrated optics devices.

References and links

1. J. Fritz, M. K. Baller, H. P. Lang, H. Rothuizen, P. Vettiger, E. Meyer, H. Güntherodt, C. Gerber, and J. K. Gimzewski, "Translating Biomolecular Recognition into Nanomechanics," Science **288**(5464), 316–318 (2000).
2. G. Wu, R. H. Datar, K. M. Hansen, T. Thundat, R. J. Cote, and A. Majumdar, "Bioassay of prostate-specific antigen (PSA) using microcantilevers," Nat. Biotechnol. **19**(9), 856–860 (2001).
3. J. D. Adams, G. Parrott, C. Bauer, T. Sant, L. Manning, M. Jones, B. Rogers, D. McCorkle, and T. L. Ferrell, "Nanowatt chemical vapor detection with a self-sensing, piezoelectric microcantilever array," Appl. Phys. Lett. **83**(16), 3428–3430 (2003).
4. L. Fadel, F. Lochon, I. Dufour, and O. Francais, "Chemical sensing: millimeter size resonant microcantilever performance," J. Micromech. Microeng. **14**(9), S23–S30 (2004).
5. G. Binnig, C. F. Quate, and C. Gerber, "Atomic Force Microscope," Phys. Rev. Lett. **56**(9), 930–933 (1986).
6. M. Tortonese, R. C. Barrett, and C. F. Quate, "Atomic resolution with an atomic force microscope using piezoresistive detection," Appl. Phys. Lett. **62**(8), 834–836 (1993).
7. M. Sepaniak, P. Datskos, N. Lavrik, and C. Tipple, "Peer Reviewed: Microcantilever Transducers: A new Approach in Sensor Technology," Anal. Chem. **74**(21), 568–575, A–575 (2002).
8. P. S. Waggoner, and H. G. Craighead, "Micro- and nanomechanical sensors for environmental, chemical, and biological detection," Lab Chip **7**(10), 1238–1255 (2007).
9. N. V. Lavrik, M. J. Sepaniak, and P. G. Datskos, "Cantilever transducers as a platform for chemical and biological sensors," Rev. Sci. Instrum. **75**(7), 2229–2253 (2004).
10. D. Raorane, S.-H. S. A. U. M. A. Lim, and A. Majumdar, "Nanomechanical Assay to Investigate the Selectivity of Binding Interactions between Volatile Benzene Derivatives," Nano Lett. **8**(8), 2229–2235 (2008).
11. J. W. Noh, R. Anderson, S. Kim, J. Cardenas, and G. P. Nordin, "In-plane photonic transduction of silicon-on-insulator microcantilevers," Opt. Express **16**(16), 12114–12123 (2008), http://www.opticsinfobase.org/oe/abstract.cfm?URI=oe-16-16-12114.
12. W. Hu, R. Anderson, Y. Qian, J. Song, J. W. Noh, S. Kim, and G. P. Nordin, "Demonstration of microcantilever array with simultaneous readout using an in-plane photonic transduction method," Rev. Sci. Instrum. **80**(8), 085101–085107 (2009).
13. K. Zinoviev, C. Dominguez, J. A. Plaza, V. J. C. Busto, and L. M. Lechuga, "A novel optical waveguide microcantilever sensor for the detection of nanomechanical forces," Lightwave Technology, Journalism **24**(5), 2132–2138 (2006).
14. J. Thaysen, A. D. Yal inkaya, P. Vettiger, and A. Menon, "Polymer-based stress sensor with integrated readout," J. Phys. D Appl. Phys. **35**(21), 2698–2703 (2002).
15. X. Yu, J. Thaysen, O. Hansen, and A. Boisen, "Optimization of sensitivity and noise in piezoresistive cantilevers," J. Appl. Phys. **92**(10), 6296–6301 (2002).
16. R. L. Gunter, R. Zhine, W. G. Delinger, K. Manygoats, A. Kooser, and T. L. Porter, "Investigation of DNA sensing using piezoresistive microcantilever probes," Sensors Journal, IEEE **4**(4), 430–433 (2004).
17. X. Yu, Y. Tang, H. Zhang, T. Li, and W. Wang, "Design of High-Sensitivity Cantilever and Its Monolithic Integration With CMOS Circuits," Sensors Journal, IEEE **7**(4), 489–495 (2007).

#117544 - $15.00 USD Received 21 Sep 2009; revised 12 Oct 2009; accepted 12 Oct 2009; published 19 Oct 2009

18. C. Kocabas, and A. Aydinli, "Design and analysis of an integrated optical sensor for scanning force microscopies," Sensors Journal, IEEE **5**(3), 411–418 (2005).
19. V. Tabard-Cossa, M. Godin, L. Y. Beaulieu, and P. Grutter, "A differential microcantilever-based system for measuring surface stress changes induced by electrochemical reactions," Sens. Actuators B Chem. **107**(1), 233–241 (2005).

1. Introduction

Micro- and nanomechanical sensors based on microcantilevers have been demonstrated as biological [1, 2], chemical [3, 4], and physical [5, 6] sensors starting in the mid-1990s [7]. Sensitivities have been reported as small as attograms for mass sensitivity and as low as 10 pg mL^{-1} for biochemical concentration sensitivity [8]. A broad range of applications in both gaseous and liquid environments have been demonstrated based on the particular receptor chemistries applied to the microcantilevers [9]. While widely recognized as highly desirable for multiplexed sensing applications, the simultaneous readout of large arrays of microcantilevers (>20) with different receptor chemistries on different microcantilevers has proven to be challenging [10].

We recently introduced an in-plane all-photonic transduction method for silicon photonic microcantilevers that is intended as a scalable transduction mechanism to enable large-scale microcantilever array sensors [11, 12]. Our transduction method utilizes a single mode waveguide embedded in a microcantilever in conjunction with a differential splitter consisting of an asymmetric multimode rib waveguide and Y-branch waveguide splitter. In our initial implementation [11] the asymmetric multimode rib waveguide is formed by depositing a 100 nm thick strip of amorphous silicon on half of the rib of a multimode rib waveguide which is placed to capture light emerging from the free end of a photonic microcantilever. Because of the asymmetric structure, the splitting ratio of the differential splitter varies as a function of the vertical position of the photonic microcantilever. We have demonstrated that a differential signal formed from the splitter's two outputs has a monotonic relationship to microcantilever deflection over a measured deflection range of ±0.5 μm. The measured sensitivity of the photonic microcantilever transduction method was 0.135×10^{-3} nm^{-1}, which is comparable to that of other readout methods currently employed for deflection-based microcantilever sensors [13–15].

Further analysis shows that sensitivity is dependent on the refractive index of the strip on the multimode rib waveguide and that the amorphous silicon strip that we previously used introduced fabrication difficulties such as delamination and deformation of the strip due to adhesion issues and intrinsic film stress. We have therefore developed a new asymmetric double-step multimode rib waveguide that replaces amorphous with crystalline silicon having a higher refractive index, which improves sensitivity while maintaining the asymmetric structure of the differential splitter and eliminating fabrication issues. Using this approach we report in this paper an improved sensitivity of 0.32×10^{-3} nm^{-1}, which is 2.4 times larger than for our previous differential splitters. Moreover, the differential splitter length is reduced by a factor of 6 from 100 μm to 17 μm, which will ultimately facilitate higher levels of integration for a given chip footprint. We also demonstrate small microcantilever arrays (<8) based on transduction with asymmetric double-step multimode rib waveguides, and examine uniformity of microcantilever readout across such arrays.

2. Design of differential splitter with double-step rib waveguide

Figure 1(a) illustrates our in-plane all-photonic transduction with the new asymmetric double-step multimode rib waveguide and a Y-branch splitter for a photonic microcantilever. The two outputs of the differential splitter are designated P_1 and P_2. The silicon photonic microcantilever has a width of 45 μm, a length of 110 μm, and a thickness of 0.65 μm and forms a single mode rib waveguide which has a rib width and height of 1.6 μm and 0.1 μm, respectively, and supports only a fundamental transverse electric (TE) mode at a wavelength of 1550 nm. Initially, the capture waveguide is a multimode rib waveguide etched 0.1 μm deep in a 0.75 μm thick silicon layer (i.e., same etch depth as the single mode waveguide) and

#117544 - $15.00 USD Received 21 Sep 2009; revised 12 Oct 2009; accepted 12 Oct 2009; published 19 Oct 2009

has a rib width of 3.0 μm. As shown in Fig. 1(b), the entire top surface of the multimode rib waveguide, except for a 1.5 μm wide section on the right half of the rib, is etched down an additional 0.1 μm to form a double-step rib waveguide. The other waveguide structures for the optical waveguide network are the same as the single mode rib waveguide in the photonic microcantilever.

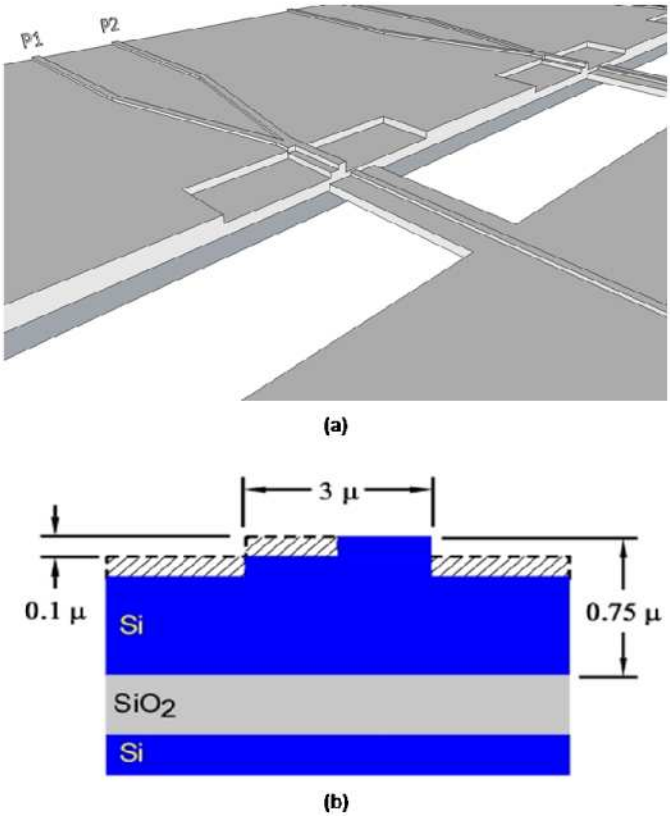

Fig. 1. (a) Schematic illustration of in-plane all-photonic microcantilever transduction structure based on a differential splitter composed of an asymmetric double-step multimode rib waveguide and Y-branch splitter. Two microcantilevers in an array are shown. (b) Cross section of the double-step rib waveguide. Dashed regions indicate the etched area from the initial multimode rib waveguide. Buried oxide layer thickness is 3 μm and the remaining silicon layer thickness is 0.55 μm.

We performed photonic simulations to optimize the length of the double-step rib waveguide in a differential splitter with results shown in Fig. 2(a). The optical output powers of the differential splitter, P_1 and P_2, vary as a function of the length of the asymmetric double-step rib waveguide. For several arbitrarily selected lengths of the waveguide, we also calculate the contrast of the differential signal. The differential signal, η, is

$$\eta = \frac{P_2 - P_1}{P_2 + P_1}, \tag{1}$$

#117544 - $15.00 USD Received 21 Sep 2009; revised 12 Oct 2009; accepted 12 Oct 2009; published 19 Oct 2009

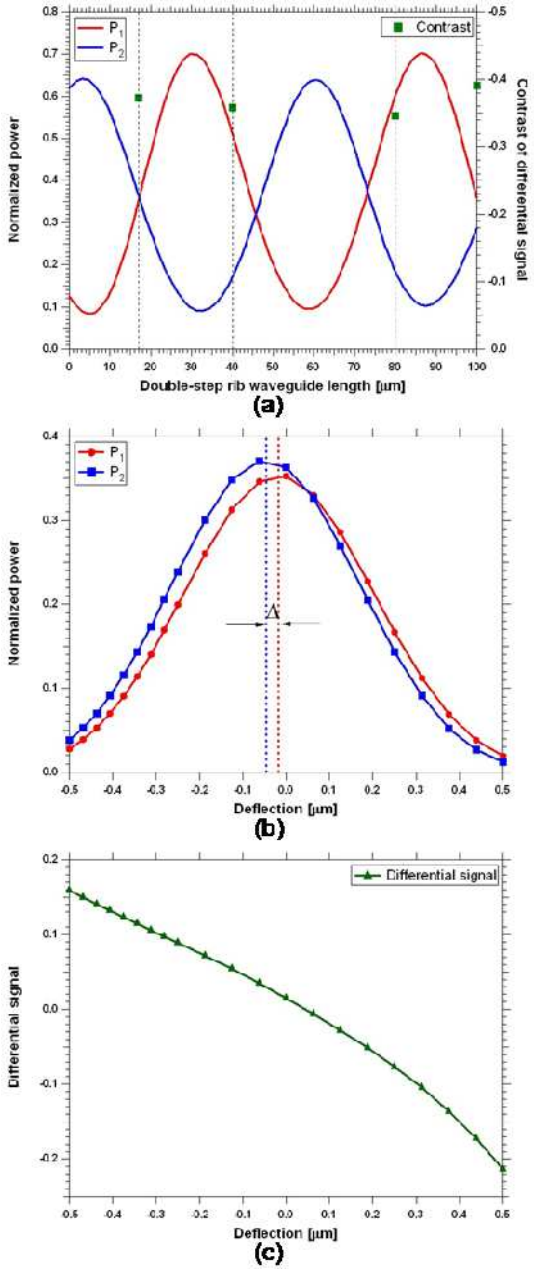

Fig. 2. (a) Normalized P_1 and P_2 output powers (left axis) and contrast of the differential signal (right axis) for selected lengths as a function of the length of the double-step rib waveguide. (b) Normalized output power and (c) differential signal as a function of deflection for a 17 μm long double-step rib waveguide.

and its contrast is the difference between the maximum and minimum values of the differential signal over the deflection measurement range (± 0.5 μm).

The important factors in choosing the length of the double-step rib waveguide are differential signal contrast, which sets the signal range, and the ratio of the peak P_1 and P_2 output powers. The latter should be close to unity such that each output signal has a similar dynamic range. Figure 2(a) suggests that the contrast variation with respect to the length of

#117544 - $15.00 USD Received 21 Sep 2009; revised 12 Oct 2009; accepted 12 Oct 2009; published 19 Oct 2009

the waveguide is not large. Therefore, we choose the shortest length (17 μm) of the asymmetric rib waveguide at which the peak output powers of P_1 and P_2 are equal. P_1 and P_2 as a function of deflection are plotted for this case in Fig. 2(b). Both P_1 and P_2 have similar Gaussian-like profiles over the deflection range of ±0.5 μm, but have a small peak offset, Δ, between the two profiles. As discussed in Ref. 11, the peak offset (in this case Δ=0.029 μm) results in a differential signal with monotonic response to deflection as shown in Fig. 2(c). The contrast of the differential signal is 0.37 which is 1.6 times greater than our previously reported design while the asymmetric rib waveguide length is 6 times shorter.

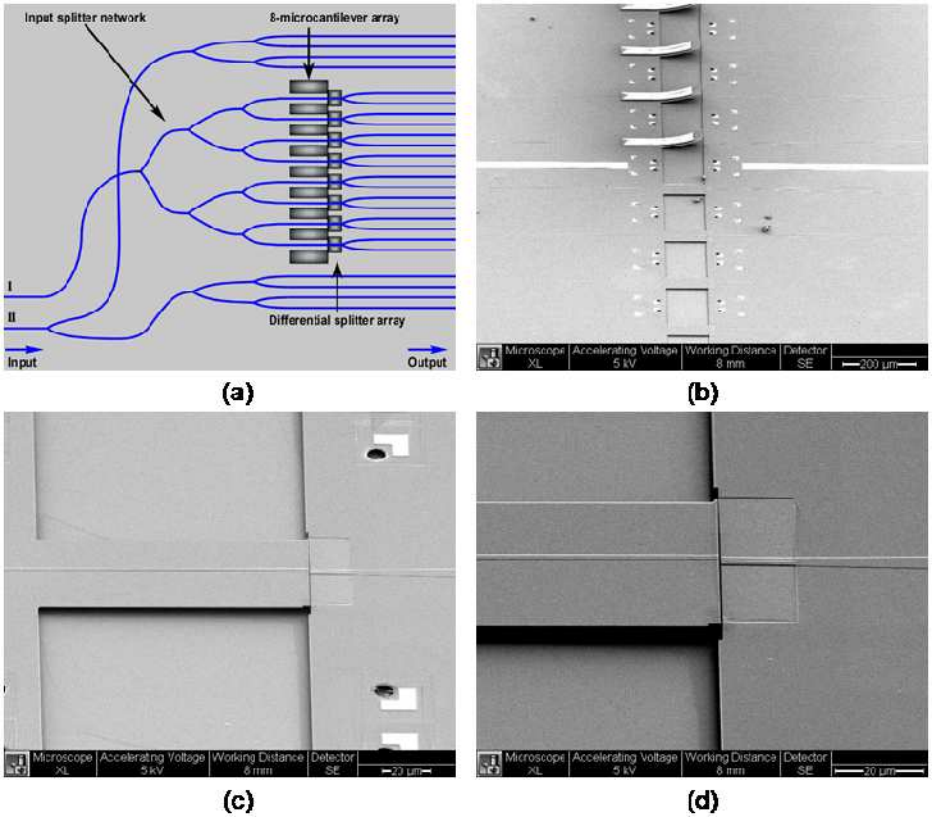

Fig. 3. (a) Schematic layout of an 8-microcantilever array with associated Y-branch input splitter network. Each fabricated die includes two such structures. SEM images of (b) an 8-microcantilever array with SU8 bending patches on the top half of the array, (c) a photonic microcantilever that is 110 μm long and 45 μm wide, and (d) a double-step rib waveguide differential splitter.

3. Fabrication of photonic microcantilever and differential splitter array system

To experimentally confirm the performance of the newly designed structure, test samples were fabricated, each with two 8-microcantilever array sets. A single array is illustrated in Fig. 3(a). In the lower left corner is the input waveguide (I) into which light from an optical fiber is butt-coupled. The input waveguide is displaced from the center of the array by a large S-bend to avoid introducing uncoupled light from the fiber into the detector array used to measure light from the differential splitter output waveguides. Light coupled into the input waveguide is split by a three stage Y branch splitter network to 8 photonic microcantilevers. Another input waveguide (II) directs light into two groups of waveguides straddling the array to facilitate alignment of detector optics prior to measuring microcantilever array photonic properties.

#117544 - $15.00 USD Received 21 Sep 2009; revised 12 Oct 2009; accepted 12 Oct 2009; published 19 Oct 2009

Fabrication of test samples is similar to what we have previously reported [11], with the exception that the asymmetric double-step rib is patterned with electron beam lithography (EBL) followed by a 100 nm etch in an inductively coupled plasma reactive ion etcher (ICP-RIE). We use EBL in a scanning electron microscope only because positioning accuracy is much better (<0.1 μm) than for our contact mask aligner (~1 μm). Figure 3(b) shows a scanning electron microscope (SEM) image of an 8-microcantilever array that has undergone the full fabrication process. Four microcantilevers (#1 through #4) are intentionally bent up with thermally stressed SU8 patches. A single microcantilever in an array is shown in Fig. 3(c) and a close-up of a double-step rib waveguide in Fig. 3(d).

4. Experimental measurement

After fabrication, samples are tested to examine the sensitivity and uniformity of the photonic microcantilever array responses as a function of deflection. The deflection state of all 8 microcantilevers in an array is simultaneously set by pushing down on them with the edge of a thin glass piece attached to a linear piezo-translator (see Ref. 12 for details of the method). The 500 μm thick glass piece is cut in the shape of an isosceles trapezoid, with a base width of 1.5 mm on the edge that makes physical contact with the 8 microcantilevers. This edge is polished to remove major defects and increase the uniformity of deflection across the array. A rotation stage and goniometer ensure that the edge of the glass piece is perpendicular to the array of microcantilevers so that all are pushed down in unison. During actuation the piezo-translator moves through a 3 μm range in 50 nm steps.

An InGaAs digital line scan camera (SU512LDV-1.7RT-0500/LSE, Goodrich) simultaneously captures light from the 16 output waveguides in an array. The output face of the sample is imaged onto the camera's linear array of pixels such that each output waveguide illuminates a single pixel. Measurements are performed for both of the 8-microcantilever arrays on a die. The Set 1 array measurement uses a camera exposure time of 0.12 ms with a corresponding line sampling rate of 3,026 Hz. Measurement for the Set 2 array uses an exposure time of 0.08 ms and a line sampling rate of 3,443 Hz. For both measurements 400 line scans are averaged to obtain the mean output power of P_1 and P_2 at each piezo-translator position. As an aside, note that use of an InGaAs line scan camera with a maximum line scan rate of approximately 4 kHz limits our detection method to measurement of static deflection rather than resonance frequency shift since typical microcantilever resonance frequencies are higher than the line scan rate.

The measured P_1 and P_2 output power from both microcantilever arrays on a single die are shown in Figs. 4(a) and 4(b) as a function of microcantilever deflection. Microcantilevers #4 and #5 of Set 1 are not included in the figures since breaks in the input waveguides prevented light from being guided to these microcantilevers. Additionally, although only four microcantilevers in each set were covered with SU8 patches, we note that most of the microcantilevers without patches were initially bent up by approximately 0.6 μm or more. The exceptions are Set 1 #8 and Set 2 #6 and #8 which have essentially no deflection after being released. This accounts for the flat P_1 and P_2 responses at positive deflection for these microcantilevers (i.e., the glass piece only contacts them near zero deflection and below). The other P_1 and P_2 profiles are Gaussian-like as expected. However, the measured profiles are wider than predicted by simulation as shown in Fig. 2(b). The difference is due to the divergence of light across the gap between the free end of the microcantilever and the capture waveguide, which is not included in the simulation. The peak power variation from waveguide to waveguide in the measured data is likely due to different losses in individual waveguides caused by factors such as dissimilar waveguide top surface conditions, coupling efficiencies at interfaces, and output waveguide facet roughness. Additionally, the peak positions of the profiles in Figs. 4(a) and (b) are not perfectly aligned because of small defects in the glass piece. Therefore, before calculating the differential signals, we redefine zero deflection for each microcantilever to be at the P_1 peak position which simulation indicates coincides with zero deflection.

#117544 - $15.00 USD Received 21 Sep 2009; revised 12 Oct 2009; accepted 12 Oct 2009; published 19 Oct 2009

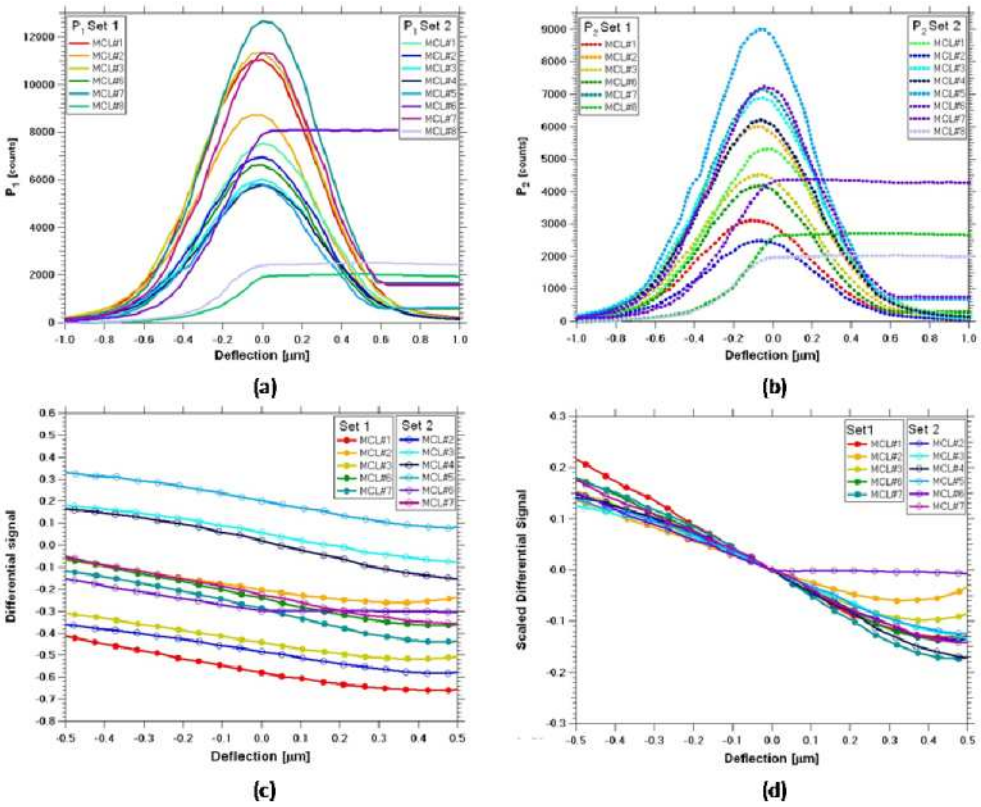

Fig. 4. Measured individual (a) P_1 and (b) P_2 output powers as a function of deflection for Sets 1 and 2. Corresponding (c) differential and (d) scaled differential signals as a function of deflection.

Figure 4(c) shows the differential signals calculated from the measured P_1 and P_2 output powers. Subsequent SEM and atomic force microscope (AFM) inspections reveal fabrication imperfections for the gaps of microcantilever #8 of Set 1 and #8 of Set 2, and a particle stuck on the tip of microcantilever #1 of Set 2. Therefore, the differential signals from these microcantilevers are not included in Fig. 4(c). Note that the differential signal curves have a wide vertical spread although their slopes are somewhat similar, making it difficult to compare differential signals for different microcantilevers in the arrays. As shown in Ref. 11, the vertical spread of the differential signals is due to different ratios of the peak values of P_1 and P_2. To compensate for the different ratios, we have introduced a scaled differential signal [12] defined as:

$$\eta_{scaled} = \frac{P_2 - \alpha \cdot P_1}{P_2 + \alpha \cdot P_1}. \qquad (2)$$

The scaling factor, α, is given by $\alpha = P_{10}/P_{20}$ where P_{10} and P_{20} are the output powers at an arbitrary reference deflection. We choose the P_1 peak position to be the reference deflection for P_{10} and P_{20}. As shown in Fig. 4(d), the scaled differential signals from 11 microcantilevers from both sets are similar for deflections of zero and below where the glass piece contacts all of the microcantilevers. As we have shown previously for differential splitters based on amorphous silicon strip loading, variation in the slopes of the scaled differential signals correlates with differences in peak offset (Δ) values [12].

#117544 - $15.00 USD Received 21 Sep 2009; revised 12 Oct 2009; accepted 12 Oct 2009; published 19 Oct 2009

5. Analysis and discussion

After SEM and AFM measurement of the as-fabricated dimensions of the asymmetric double-step rib waveguides, we re-ran the simulation of its photonic response as a function of deflection. The updated simulation results are compared with the average measured scaled differential signal in Fig. 5.

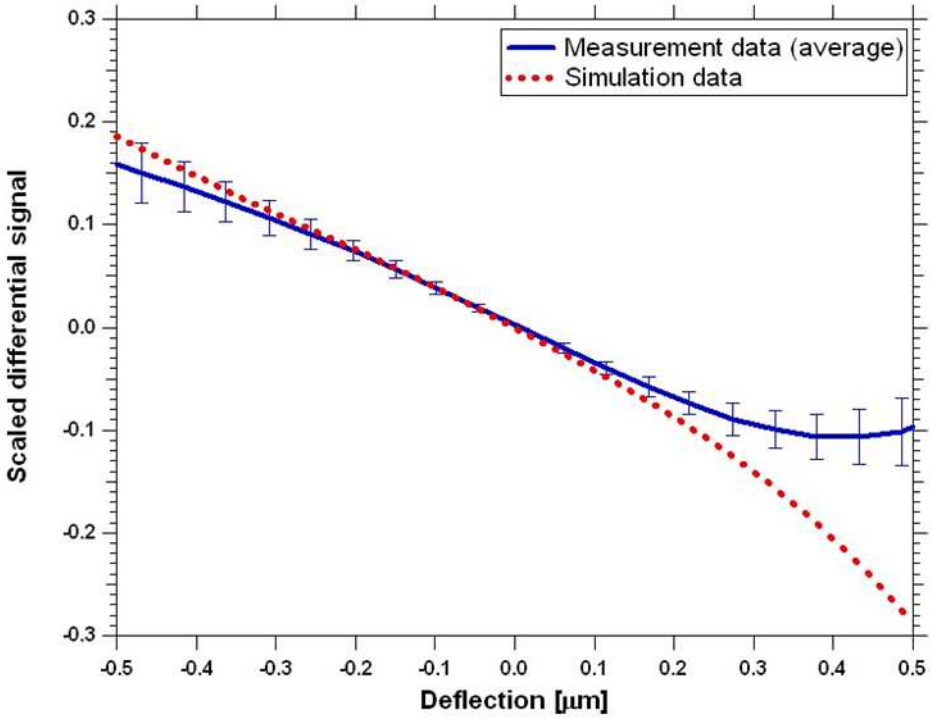

Fig. 5. Comparison of measured data with simulation results

Over the deflection range where the averaged scaled differential signal exhibits a relatively linear behavior, roughly –0.5 μm to 0.3 μm, the average slope is –0.32 μm^{-1}. The difference between measurement and simulation in that deflection range is from the broader widths and a slightly larger peak offset of the measured P_1 and P_2 profiles. While the averaged scaled differential signal agrees well with the simulation in that range, the two curves diverge noticeably for deflections greater than 0.3 μm (we note that microcantilever #6 from Set 2 is not included in the average for deflections greater than zero and hence does not bias the average in this region). Analysis of measurement data indicates that this is mainly due to a background DC offset in the measurements. Although an aperture mask is used to block the majority of stray light not associated with the P_1 and P_2 outputs, some amount of scattered and stray light is still incident on the InGaAs camera's pixel array. Because of the scattered and stray light, the camera measures a DC offset in addition to the deflection-dependent output powers. In the region where P_1 and P_2 have large values, such as around zero deflection, the effect of the background DC offset on the scaled differential signal is negligible. However, when the DC offset is comparable to the values of P_1 and P_2, the scaled differential signal will differ markedly from the expected behavior. The effect is more pronounced for positive deflections because the P_2 peak is shifted toward the negative deflection region. Since the effect is noticeable only for deflections greater than 0.3 μm, the practical implication of the DC offset is a limitation of the dynamic range of the microcantilevers. As the intended future use of the photonic microcantilevers is for biological and chemical sensing scenarios where the expected static deflection is on the order of 100 nm [9], we do not expect the DC offset to cause a significant limitation to sensing. Nonetheless, we are presently investigating

#117544 - $15.00 USD Received 21 Sep 2009; revised 12 Oct 2009; accepted 12 Oct 2009; published 19 Oct 2009

techniques to dramatically reduce stray light in the silicon slab to largely eliminate the DC offset issue.

Two important parameters for characterizing the capability of a microcantilever sensor to detect small changes in static deflection are the sensitivity and the minimum detectable deflection (MDD). The sensitivity of a microcantilever sensor is the change in output signal per unit deflection of the microcantilever. As noted above, the average sensitivity is 0.32×10^{-3} nm^{-1}, which is orders of magnitude better than piezoresistive readout methods [14, 16, 17] (with sensitivities typically on the order of 10^{-6} nm^{-1}), and comparable to optical lever readout methods [13, 18] whose best reported sensitivities are on the order of 10^{-3} nm^{-1} [18]. The MDD gives the limit of detection of microcantilever deflection and is calculated by dividing the noise of the transduction signal by the sensitivity of the readout method [13]. For our photonic microcantilevers, the noise of the scaled differential signal ($\delta\eta$) can be determined from the measured power, noise, and correlation of the P_1 and P_2 outputs for each microcantilever. The first-order approximation of the noise of the scaled differential signal is given by:

$$\delta\eta = \frac{2\alpha}{\left(P_2 + P_1\right)^2}\sqrt{P_2^{\,2}\delta P_1^{\,2} + P_1^{\,2}\delta P_2^{\,2} - P_1P_2\delta P_1\delta P_2 r_{12}}\,, \tag{3}$$

where δP_1 and δP_2 are the measured noise of the two outputs and r_{12} is the correlation coefficient for P_1 and P_2. Based on the measured values of P_1 and P_2 and the slope of the scaled differential signal, we obtain an average MDD of 141 pm for a 3.5 Hz bandwidth, which corresponds to a minimum detectable surface stress of 0.3 mN/m. Note that this is three orders of magnitude smaller than the microcantilever spring constant, which is measured to be 0.3 N/m. The MDD is comparable to or better than other common readout methods [14, 16, 17, 19] for static deflection. Analysis of the total noise shows that the signal shot noise is roughly equal in magnitude to that of the combined power-independent noises - thermal noise, dark current shot noise, flicker noise, etc. The MDD can be improved by increasing the output powers, which will reduce $\delta\eta$, and by decreasing the exposure time, which will reduce the dark current shot noise.

6. Conclusion

In summary, we have implemented a new differential splitter using an asymmetric double-step multimode rib waveguide for in-plane all-photonic transduction of a photonic microcantilever. Simultaneous measurement of an array of microcantilevers using this transduction method has been demonstrated with mechanical actuation of the microcantilevers. From the measured outputs, the scaled differential signals are calculated and 11 of the 16 microcantilevers from two independent arrays show acceptable uniformity and repeatability. The averaged scaled differential signal from the measurements is well matched with simulation in the deflection range of –0.5 μm to 0.3 μm with noticeable disagreement for deflections greater than 0.3 μm due to a DC offset in the measurements. The sensitivity and MDD of the photonic microcantilever system are 0.32×10^{-3} nm^{-1} and 141 pm, respectively, which are comparable to or better than other common readout methods for nanomechanical static-deflection sensors. Currently we are investigating further structure optimization to enhance system performance and practical methods to eliminate the measured DC offset. We are also pursuing application of the transduction method reported here to much larger arrays of photonic microcantilevers.

Acknowledgment

This work was supported in part by NSF grants ECS-0602261 and IIS-0641973, and DARPA grant 66001-04-8933.

#117544 - $15.00 USD Received 21 Sep 2009; revised 12 Oct 2009; accepted 12 Oct 2009; published 19 Oct 2009